Ultrasound in Med. & Biol., Vol. 28, No. 9, pp. 1165–1172, 2002

0301-5629/02/$–see front matter

PII: S0301-5629(02)00567-7

● *Original Contribution*

A NEW ULTRASOUND INSTRUMENT FOR *IN VIVO* MICROIMAGING OF MICE

F. S. FOSTER,*§ M. Y. ZHANG,* Y. Q. ZHOU,† G. LIU,‡ J. MEHI,‡ E. CHERIN,* K. A. HARASIEWICZ,* B. G. STARKOSKI,‡ L. ZAN,‡ D. A. KNAPIK‡ and S. L. ADAMSON†

*Sunnybrook and Women's College Health Sciences Centre, and §Mouse Imaging Centre at the Hospital for Sick Children, Departments of Medical Biophysics, Ob/Gyn, Physiology, University of Toronto, Toronto, Ontario, Canada; †Samuel Lunenfeld Research Institute at Mount Sinai Hospital, Toronto, Ontario, Canada; and ‡VisualSonics Inc., Toronto, Ontario, Canada

(*Received* 7 *January* 2002; *in final form* 7 *June* 2002)

Abstract—We report here on the design and evaluation of the first high-frequency ultrasound (US) imaging system specifically designed for microimaging of the mouse. High-frequency US or US biomicroscopy (UBM) has the advantage of low cost, rapid imaging speed, portability and high resolution. In combination with the ability to provide functional information on blood flow, UBM provides a powerful method for the investigation of development and disease models. The new UBM imaging system is demonstrated for mouse development from day 5.5 of embryogenesis through to the adult mouse. At a frequency of 40 MHz, the resolution voxel of the new mouse scanner measures 57 μm × 57 μm × 40 μm. Duplex Doppler provides blood velocity sensitivity to the mm per s range, consistent with flow in the microcirculation, and can readily detect blood flow in the embryonic mouse heart, aorta, liver and placenta. Noninvasive UBM assessment of development shows striking similarity to invasive atlases of mouse anatomy. The most detailed noninvasive *in vivo* images of mouse embryonic development achieved using any imaging method are presented. (E-mail: stuart.foster@swchsc.on.ca)

Key Words: **Ultrasound, High frequency, Biomicroscopy, Mouse imaging, Phenotyping, Mouse development, Disease models.**

INTRODUCTION

As human and mouse genetic sequencing projects near completion, the next and greater challenge will be to define the roles of tens of thousands of genes in the context of complex organisms (Burley et al. 1999; Clark 1999; Bentley 2000). The mouse has emerged as one of the models of choice (Marshall 2000) for such studies. Not only do we share over 90% of our genes with the mouse, but this mammal is prolific and inexpensive to house. Over the past several decades, researchers have studied naturally occurring mutations and have learned to manipulate the mouse genome in a targeted and predictable fashion using transgenes and knockouts (Battey et al. 1999). In addition, large-scale random chemical mutagenesis studies (Hrabe de Angelis et al. 2000) are being conducted to identify novel genes involved in human diseases. Thus, there is a significant need for rapid, high-throughput tests to screen for critical geneotype-phenotype relationships. New screening methodologies will include rapid methods for behavioral analysis, automated physiological screens and systems for biochemical profiling of blood and urine. A variety of optical and nonoptical imaging techniques, including US biomicroscopy (UBM), magnetic resonance (MR) microscopy, computed tomographic (CT) microscopy and positron emmision tomography (PET) will be added to this list because they are likely the only means of acquiring anatomic and spatially mapped functional information about living animals. Although UBM does not provide molecular specificity, it has the advantage of low cost, rapid imaging speed, portability and high resolution.

Several groups have actively conducted mouse imaging research using diagnostic US instrumentation operating in the 7.5- to 12-MHz frequency range where resolution is on the order of 300 to 500 μm (Fentzke et al. 1997, 1998; Mor-Avi et al. 1999; Scherrer-Crosbie et al. 1998, 1999). Investigations of mouse models of myocardial infarction have been performed using contrast agents (Scherrer-Cros-

Address correspondence to: Dr. F. S. Foster, Dept. of Medical Biophysics and University of Toronto, Sunnybrook and Women's College Health Sciences Centre, Rm S-658, 2075 Bayview Ave, Toronto, Ontario M4N 3M5 Canada. E-mail: stuart.foster@swchsc.on.ca

bie et al. 1999) and studies of mouse right ventricular function have been undertaken using transesophageal imaging (Scherrer-Crosbie et al. 1998). It has also been possible to examine transgenic models of cardiac hypertrophy with some success (Fentzke et al. 1998). Applications of conventional phased-array US in the mouse will undoubtedly continue to improve as array transducers and signal processing in these systems are moved to higher frequencies. Although conventional US can, in some cases, provide useful information, resolution is marginal and useful observations of neonates and embryonic development are all but impossible. Scaling diagnostic US instruments for applications in the mouse requires several important modifications. In terms of linear dimensions, the most obvious requirement is the need for a scaling factor of approximately 10. For example, the mouse heart measures about 10 to 12 mm on the long axis, whereas the human heart measures approximately 12 to 15 cm. The ratio of the dimensions of other mouse organs to human organs is similar. Optimal imaging of the mouse, therefore, requires an approximately 10-fold improvement in resolution if the same level of structural detail within organs is to be observed. Because resolution scales directly with frequency, the required level of resolution can be achieved by employing much higher US frequencies in the 20 to 60 MHz range. Specialized scanning systems (US biomicroscopes) operating in this frequency range have recently become available for applications in clinical imaging of the eye and skin and in intravascular imaging (Foster et al. 2000c; Pavlin and Foster, 1995; Silverman et al., 1997). UBM has also been tested as a tool for mouse imaging (Foster et al. 2000c; Turnbull 1999; Aristizabal et al. 1998; Srinivasan et al. 1998; Turnbull et al. 1995, 1996). Turnbull et al. (1995) first reported the use of UBM to observe mutant phenotyping in the mouse embryo. Since that time, improvements in the technology have permitted numerous other investigations in the mouse to be performed (Foster et al. 2000c) using prototype scanners built in our laboratory. In particular, the development of high-frequency continuous-wave (CW) (Christopher et al. 1996), pulsed-wave (PW) (Christopher et al. 1997), and color Doppler (Kruse et al. 1998; Goertz et al., 2000) have enabled the measurement and characterization of the microcirculation to be achieved. Another important innovation has been the development of methodologies for the guided injection of genetic material to specific sites in the developing mouse embryo (Liu et al. 1998).

The technical advances of the past few years have now been consolidated into a new US mouse imaging system that has recently become commercially available (VisualSonics VS40, Toronto, Ontario, Canada). In this report, the design criteria of the new scanner and its performance in noninvasive *in vivo* real-time mouse imaging are described. This scanner is unique in that it provides frequency selectivity over the range from 19 to 55 MHz, corresponding, respectively, to lateral resolutions ranging from 100 to 60 μm. For the first time, in this frequency range, the scanner combines imaging and Doppler blood flow sensing. Performance issues such as resolution and blood velocity sensitivity are described. Relevant applications in the mouse are given with images from day 5.5 of embryogenesis to adulthood. These images demonstrate the broad range of potential biologic applications of this novel imaging technology.

INSTRUMENT DESIGN

Figure 1a shows a schematic diagram of high-frequency US mouse imaging. The imaging system consists of a 3-D micropositioning scanhead that scans a high-frequency transducer over the field of view plus the associated signal- and imaging-processing hardware. The imaging process has been previously described in detail (Foster et al. 2000c). For mouse imaging, the 19- to 55-MHz center frequency transducer is moved linearly over the imaging field (8 mm $\times$ 8 mm), collecting US data at equally spaced lines (10 to 20 μm between lines is typical), as shown in Fig. 1a. US echo signals from the transmitter–receiver are nonlinearly processed to enhance low level signals, detected, and converted from analog to digital format before scan conversion. A PC running Windows® NT controls system timing, motion control, scan conversion and display. A photograph of the system and a high-resolution grey-scale image of a day 13.5 mouse embryo are shown in Figs. 1b and c, respectively. Pulsed Doppler processing is based on the design of Christopher et al. (1997) and implemented in a duplex configuration.

The transducer is a key enabling technology. We have previously developed a wide range of transducers for the 20- to 80-MHz range based on the ferroelectric polymer poly vinyledene fluoride and have employed variants of these devices in the new scanner (Foster et al. 2000b; Sherar and Foster 1989).

In US, a trade-off between frequency (resolution) and depth of penetration is always made. The nomogram of Fig. 2a summarizes this trade-off for the mouse imaging system. The selectable frequency range of the scanner (19 to 55 MHz) corresponds to maximum imaging depths of approximately 15 mm and 5 mm, respectively. Exact penetration limits are determined by the attenuation properties of the tissues being imaged. The resolution of the imaging system depends on many factors, including the frequency and bandwidth of the US pulse, the geometry of the transducer, peak transmitted pressure and tissue-attenuation properties. The standard transducer used with the new mouse imager is a 3-mm diameter 40-MHz center frequency device with a focal length of 6 mm. The large bandwidth of this polymer transducer (120%) (Foster et al. 2000c) enables it to be effectively operated over a range of center frequencies from

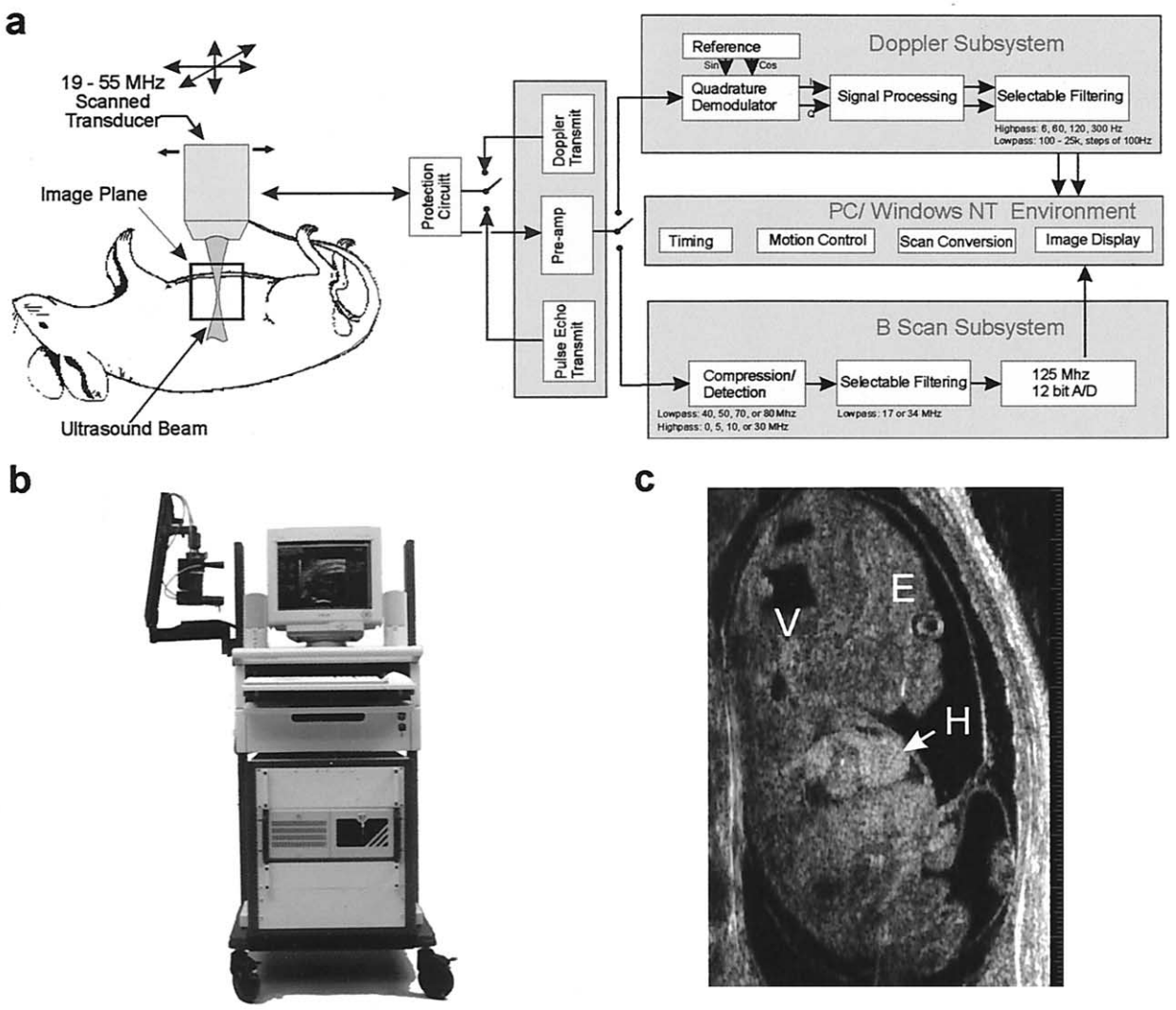

Fig. 1. (a) Schematic of a 20- to 55-MHz US biomicroscope (UBM) for mouse imaging. The high-frequency transducer is mechanically scanned over the mouse tissues of interest to generate B-scan images and duplex Doppler waveforms. System timing, motion control, scan conversion and image display are performed in a Windows® NT environment. Imaging and Doppler signals returned from the tissue are processed in separate subsystems before conversion for display. (b) Photograph of complete system. Note that the 3-D micropositioned scanhead is supported by an arm attached to the imaging console. (c) Example image plane of a longitudinal section of a 13.5-day-old mouse embryo showing the developing eye (E), lateral ventricle (V) and heart (H). Smallest scale divisions are 100 μm.

19 to 55 MHz. Table 1 provides a comparison between theoretically predicted and measured resolution for the standard 40-MHz probe operated at 20-, 25-, 40- and 55-MHz settings on the scanner. The theoretical and experimental measurements of Table 1 are performed for the linear portion of the US beam by filtration (−6-dB bandpass centered at the measured center frequency). Theoretical lateral resolution of the linear beam at the focal point is given by:

$$R_{lat} = \lambda \cdot f\text{-}number \quad (1)$$

where λ is the wavelength at the fundamental center frequency and *f*-number is the ratio of the focal length to the diameter of the transducer. Experimental field measurements were performed with a custom Agilent hydrophone with a spot size of 25 μm. and band width extending from 1 to above 60 MHz. With these restrictions, excellent agreement between experiment and theory is obtained, as shown in Table 1. Resolution of linear beams ranges from approximately 100 μm at 20 MHz to approximately 60 μm at 55 MHz center frequencies. Table 1 shows that the excitation frequencies of the

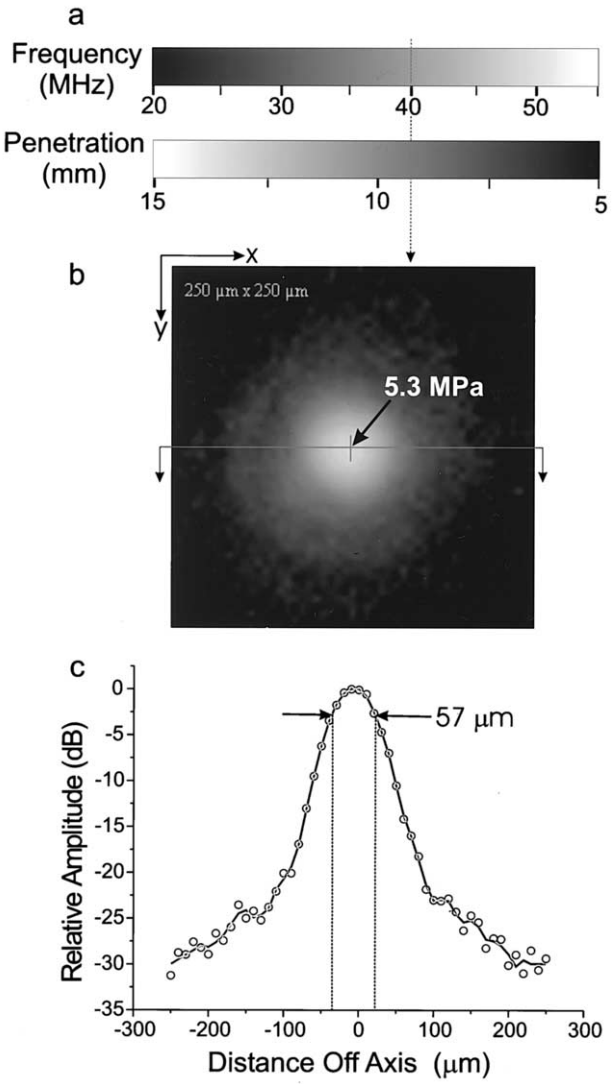

Fig. 2. (a) Nomogram of the US frequency–penetration tradeoff. At 40 MHz, penetration of approximately 8 mm can be achieved. (b) The spatial distribution of US pressure from a 40-MHz US transducer perpendicular to the direction of propagation at the beam focus. The measured peak pressure at the center of the distribution is 5.3 MPa (0 dB). (c) Plot of relative pressure amplitude through the center of the beam. The scanner lateral resolution calculated from this beam profile is 57 μm. Axial resolution is determined by the physical length of the US pulse. In this case, it is approximately 40 μm.

transducer are not identical to the actual transmitted pulse frequency measured by the hydrophone at the focus. The latter are determined by the electromechanical properties of the transducer and the electrical matching of the probe to the front end electronics. Nonlinear propagation also plays an important role in defining the actual frequency content of the pulse, as described by (Cherin et al. 2002).

Table 1. Lateral resolution and operating frequencies

Transmit frequency (MHz)	Fundamental center frequency at focus (MHz)	Theoretical beam width (μm)	Measured beam width (μm)
19	29	104.4	102
25	34	88.2	92
40	44	68.2	72
55	48	62.5	63.5

The scanner provides a series of radiofrequency (RF) filters to set the receive band width. Low-pass filters of 40, 50, 70 and 80 MHz set the upper boundaries and high-pass filters of 0, 5, 10 and 30 MHz set the lower boundaries. Thus, the user has significant control over the system band width and, hence, the resolution achieved in imaging. In particular, nonlinear propagation will act to enhance beam quality (Cherin et al. 2002). If the filters are left as wide as possible (0 to 70 MHz), resolution at a given operating frequency will be improved over the numbers quoted in Table 1. For example, using the 40-MHz operating frequency with the filters wide open, we see in Fig. 2b and c that an excellent focal distribtion is obtained. A 2-D map of the spatial pressure sensitivity (Fig. 2b) shows a symmetrical distribution with a peak pressure of 5.3 MPa at the focus. In terms of beam propagation, this is well into the nonlinear region. The width of the pressure distribution at –3 dB corresponds to the pulse echo lateral resolution. In this case, the lateral pulse-echo resolution is 57 μm, as shown in Fig. 2c.

Resolution in the axial dimension is governed by the compactness of the pressure pulse which, in turn, is related to the band width of the transducer and processing electronics. An approximate expression for axial resolution is:

$$R_{ax} = c/(2 \cdot BW) \quad (2)$$

where BW is the −6-dB band width of the received US pulse. At 40 MHz, with BW = 25 MHz, the axial resolution is approximately 30 μm.

Pulsed Doppler processing is used to probe the hemodynamics of the mouse circulatatory system. Using a typical duplex Doppler configuration, the image is used to identify vessels or cardiac structures, and a sample volume placed interactively on the target structure. The pulsed Doppler system then returns the Doppler waveform for that location (after angle correction). The minimum detectable velocity depends on many factors, such as the Doppler angle, the ratio of blood scatter to tissue scatter, clutter arising from tissue motion and signal sampling as dictated by the pulse-repetition frequency (PRF). The minimum detectable velocity of the mouse UBM is on the order of 1 mm/s, consistent with blood velocities in the microcircula-

tion (Christopher et al. 1997; Goertz et al. 1998). At present, the maximum PRF is 25 kHz, corresponding to a maximum detectable velocity of 23.5 cm/s at zero Doppler angle and 40 MHz.

B-mode imaging can be performed at 2 to 8 frames/s, sufficient for many applications. The scanhead provides micropositioning of the transducer in 3-D. One axis provides rapid imaging motion and the other two axes allow repositioning of the scan plane for sequential image plane acquisitions. Positioning accuracy is plus or minus 2 μm in the imaging direction and plus or minus 6 μm in the other two directions. The depth of field of the final images can be improved by taking several images at different depths and stitching the focused regions together; we refer to this as zone focusing. Additional details on scanner design are given in references (Deng et al. 1998; Passmann and Ermert 1994; Sherar et al. 1989; Foster et al. 1993; Lockwood et al. 1996).

EXPERIMENTAL PROTOCOL FOR MOUSE IMAGING

All animal experimentation was performed under an approved animal care protocol. Timed pregnant CD-1 mice at various stages of development were lightly anesthetized with enflurane and imaged on a special mouse imaging stage that provided temperature feedback and heart rate monitoring (THM100 Indus Instruments, Houston, TX). After being anesthetized, the mouse abdomen was shaved and further cleaned with a chemical hair remover to minimize US attenuation. Imaging was performed while maintaining the mouse temperature between 36 and 38°C, with US gel as a coupling fluid on the skin. This procedure was carried out 1 to 3 times on each mouse, with at least 24 h between imaging sessions. Special care was taken with neonates to gently restrain their fragile bodies and regulate temperature. The procedure on each neonate took no more than 1 h, but studies with adults or embryos could extend to 2 h.

RESULTS

Examples of images made during early to mid mouse embryo development are given in Fig. 3. Figure 3a shows the earliest detection of the conceptus at day 5.5 of embryogenesis. At this stage, the inner cell mass (ICM), composed of the epiblast and primitive endoderm, and the trophectoderm have begun to form a cylindrical embryo. The embryo is visible as a diffuse bright region of approximately 250 μm in diameter in the lumen of the uterus. By day 7.5, the embryo has developed three distinct cavities

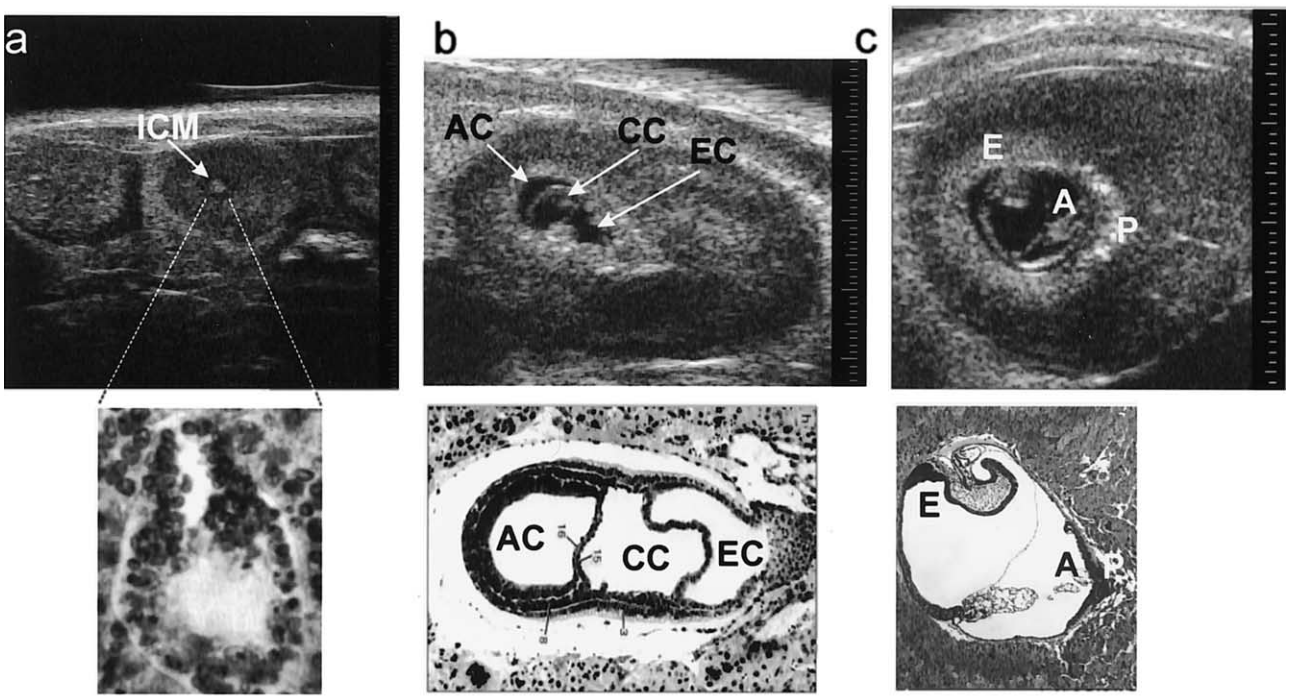

Fig. 3. Early development of the mouse embryo: (a) day 5.5, showing a bright region central in the uterus that represents the inner cell mass (ICM) and associated cells of this embryo. (b) day 7.5, showing the three cavities of the embryo: the amniotic cavity (AC), the coelomic cavity (CC), and the ectoplacental cavity. (c) day 8.5, showing the now visible embryo as well as the allantois (A) adjacent to the developing placenta (P). Small division: 100 μm. Histology in (a), (b) from Kaufman (1999), with permission.

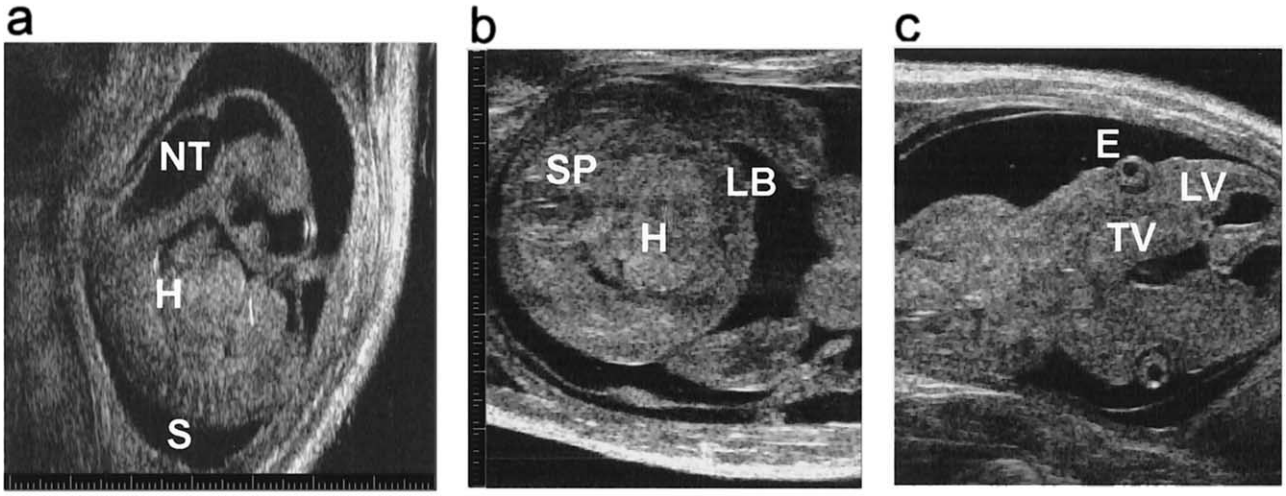

Fig. 4. *In vivo* UBM images of mouse embryo anatomy at mid gestation: (a) day 11.5 embryo in longitudinal section showing the neural tube (NT), heart (H) and primitive developmental units called somites (S). (b) day 13.5 embryo in transverse section showing development of the limb buds (LB), heart (H) and spine (SP). (c) day 13.5 embryo in oblique section showing the third ventricle (TV) and the superior horns of the lateral ventricles (LV). The eyes (E) are also visible in this section. Images were formed using a zone focusing method as described in the text. Small scale divisions: 100 μm.

(Fig. 3b): the amniotic cavity (AC), the coelomic cavity (CC), and the ectoplacental cavity (EC).

At day 8.5 (Fig 3c), the embryo (E) is clearly visible wrapping around the amniotic cavity and the allantois (A) is evident. Excellent correlation between the US images and histological sections is observed. Images obtained past midgestation are given in Fig. 4. At day 11.5, a longitudinal view of the embryo (Fig. 4a) can be used to measure crown-rump length (in this case 6.2 mm). Also visible are the beating heart, the neural tube and developing somites in the tail region. Transverse images made at day 14.5 (Fig 4b) depict the chest in cross-section with the heart (H), forelimb buds (LB) and the spine (SP). This plane also traverses the lower mandible on the right side of the image. A third image (Fig. 4c) at day 14.5 shows an oblique section through the brain and torso. Visible are early eye development (E), the third ventricle (TV), and the superior horns of the lateral ventricles (LV). A longitudinal view of the lower abdominal region of a 1.5-day-old neonate is shown in Fig. 5a. Visible are the liver (L), spleen (S), bladder (B), kidney (K) and spine (SP). Examples of images of adult mouse liver and kidney made with the VisualSonics system are

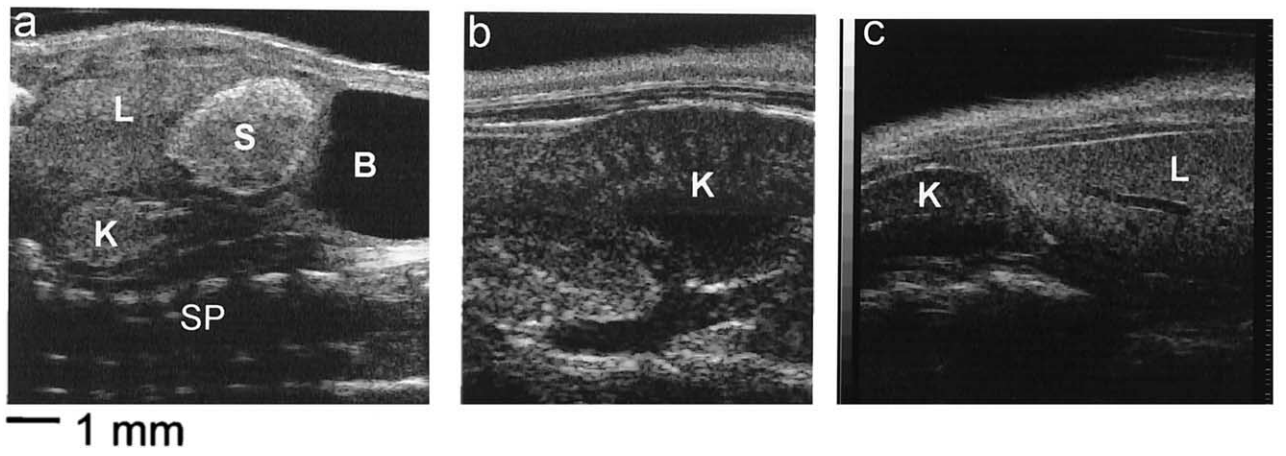

Fig. 5. (a) 1.5-day-old neonate longitudinal section showing the liver (L), kidney (K), spleen (S), spine (SP) and bladder (B). (b) Composite longitudinal section of an adult mouse kidney made at 55 and 25 MHz. The transition point is midway down in the image. (c) Oblique section through the liver (L) and kidney (K) of an adult mouse showing an hepatic vein.

shown in Figs. 5b and c. These oblique sections reveal structure remarkably similar to that seen in images of human organs taken at much lower frequencies. Visible are the collecting structures of the kidney, as well as hepatic veins and other fine structure in the liver. The kidney image of Fig. 5b is a composite in which the near field was made at 55 MHz and the far field was made at 25 MHz. The segmental anatomy of the kidney is visible.

The use of Doppler signal processing enables us to examine details of flow velocities in the heart and other organs. The Doppler waveform produced by placing the sample volume in the mitral orifice of a 12.5-day-old mouse embryo is given in Fig. 6a. Here, the Doppler angle is close to 0° and the frequency is 40 MHz, so that the peak velocity of this waveform is approximately 180 mm/s. Properly regulated blood flow from the placenta to the developing embryo is vital for normal development. It is possible to visualize the placenta throughout embryonic development and to measure both arterial and venous flow velocities. Figure 6b shows a 40-MHz UBM Doppler image of flow in the umbilical chord at day 16.5 with a Doppler sample volume positioned to record both forward (arterial) and reverse (venous) flow. Note the strong Doppler signal with clear separation of both arterial and venous components. Again, the Doppler angle, θ, is close to 0°, resulting in a peak arterial velocity of 32 mm/s and relatively constant venous flow with a velocity of 19 mm/s. Doppler waveforms of aortic and renal arteries recorded from day 1.5 neonates are shown in Figs. 6c and d, respectively. These waveforms, obtained at near normal incidence to keep the peak velocities within range, show distinctly different pulse shapes, reflecting the variation in vascular impedance faced by each.

DISCUSSION AND CONCLUSION

US imaging has been scaled and optimized for the visualization of the living mouse. The resulting US biomicroscope has axial resolution on the order of 40 μm and lateral resolution ranging from 57 μm to 104 μm, depending on the choice of frequency. The current scanner (VisualSonics VS40) provides a field of view of 8 mm $\times$ 8 mm with a frame rate up to 10 Hz. The mouse UBM has the advantage of low cost, rapid imaging speed and portability. Real-time high-resolution imaging in combination with the ability to provide functional information on blood flow *via* pulsed Doppler provides a powerful combination for the investigation of normal development and disease models. One of the most important advantages of noninvasive imaging is the ability to image tissue in the living state where normal tissue dynamics and physiological processes are intact. This results in a unique opportunity to explore development and models of human disease in longitudinal studies where animals are not necessarily sacrificed at each time point. Images made with the new UBM show the ability to study mouse development from about day 5 of embryogenesis to adulthood, as demonstrated in Figs. 3–6. Significant image contrast is seen between the fluid-filled spaces, such as the amniotic cavity, the neural tube and brain ventricles and surrounding soft tissues. Certain tissues, such as the lens of the eye (Fig. 4c), are also highly contrasted, but blood is not hypoechoic as it is at low frequencies. This complicates the differentiation of the heart wall from the blood pool (*e.g.*, Fig. 4b) at certain stages of development. Images of soft tissues, such as liver and kidney, in the neonate and adult bear a striking similarity to human US imaging at lower frequencies and larger scales. The high backscatter from blood has one advantage, in that it provides a type of spontaneous contrast that improves the detectability of the vasculature. Doppler examination of the developing heart and placenta reveal flow hemodynamics difficult or impossible to obtain by other means. The flow wave-

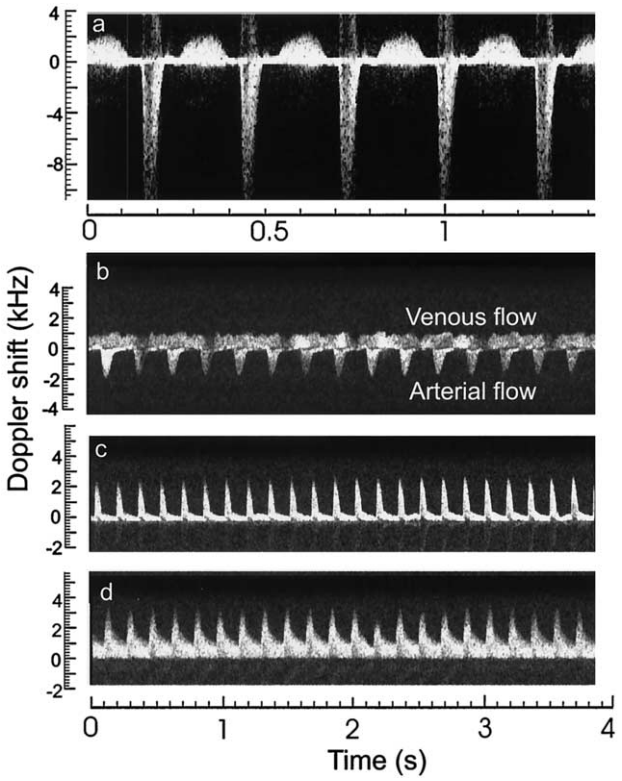

Fig. 6. Doppler waveforms: (a) Flow through the mitral orifice at day 12.5 of gestation. (b) Umbilical artery and vein at day 16.5 of gestation. Peak arterial and venous flow velocities calculated from the Doppler equation are 32 mm/s and 19 mm/s respectively. (c) Aortic waveform in a 1.5-day-old mouse neonate showing strong pulsitility, and (d) renal artery waveform in a 1.5-day-old neonate showing the markedly damped characteristic associated with the low resistance of the renal vascular bed.

forms for the mouse aorta and right renal artery in the neonate also bear a strong resemblance to human waveforms, except for the high heart rate. Both anatomic and Doppler measures should provide utility for rapid phenotyping of either targeted or random gene mutations.

In terms of disease modeling, UBM mouse imaging will permit longitudinal studies of disease progression, as well as studies of novel treatment strategies. A good example of this is the development and evaluation of new antiangiogenesis drugs for cancer treatment using UBM imaging and Doppler (Foster et al. 2000a). Future generations of this equipment will incorporate many new features, such as linear phased arrays with no moving components, high frame-rates, and advanced 3-D image analysis programs, allowing much more rapid and quantitative evaluation of mouse development, phenotype and response to treatment.

Acknowledgments—The authors acknowledge the financial support of the Canadian Institutes of Heath Research, the National Cancer Institute of Canada, the Terry Fox Foundation, and the Richard Ivey Foundation. Y. Q. Zhou acknowledges the personal support of the Ontario Research and Development Challenge Fund. The authors are grateful to Yong Lu for assistance with histology. F. S. Foster also wishes to acknowledge and disclose a financial interest in VisualSonics, the company now making this technology available to other researchers.

REFERENCES

Aristizabal O, Christopher DA, Foster FS, Turnbull DH. 40 MHz echocardiography scanner for cardiovascular assessment of mouse embryos. Ultrasound Med Biol 1998;24:1407–1417.

Battey J, Jordan E, Cox D, Dove W. An action plan for mouse genomics and genetic resources. Nature Genet 1999;21:73–75.

Bentley DR. The human genome project—An overview. Med Res Rev 2000;20:189–196.

Burley SK, Almo SC, Bonanno JB, et al. Structural genomics: Beyond the human genome project. Nature Genet 1999;23:151–157.

Cherin EW, Poulsen JK, van der Steen AW, Foster AW. Experimental characterization of fundamental and second harmonic beams for a high frequency ultrasound transducer. Ultrasound Med Biol 2002; in press.

Christopher DA, Burns PN, Foster FS. High frequency continuous wave Doppler ultrasound system for the detection of blood flow in the microcirculation. Ultrasound Med Biol 1996;22:1196–1203.

Christopher DA, Starkoski BG, Burns PN, Foster FS. High frequency pulsed Doppler ultrasound system for detecting and mapping blood flow in the microcirculation. Ultrasound Med Biol 1997;23:997–1015.

Clark MS. Comparative genomics: The key to understanding the human genome project. Bioessays 1999;21:121–130.

Deng CX, Lizzi FL, Silverman RH, Ursea R, Coleman DJ. Imaging, and spectrum analysis of contrast agents in the in vivo rabbit eye using very-high-frequency ultrasound. Ultrasound Med Biol 1998; 24:383–394.

Fentzke RC, Korcarz CE, Lang RM, Lin H, Leiden JM. Dilated cardiomyopathy in transgenic mice expressing a dominant-negative CREB transcription factor in the heart. J Clin Invest 1998;101: 2415–2426.

Fentzke RC, Korcarz CE, Shroff SG, et al. Evaluation of ventricular and arterial hemodynamics in anesthetized closed-chest mice. J Am Soc Echocardiog 1997;10:915–925.

Foster FS, Burns PN, Hope-Simpson D, et al. Ultrasound for the visualization and quantification of tumour microcirculation. Cancer Metast Rev 2000a;19:131–138.

Foster FS, Harasiewicz KA, Sherar MD. Medical and biological imaging with polyvinylidene fluoride (PVDF) transducers. IEEE Trans Ultrason Ferroelec Freq Control 2000b;47:1363–1371.

Foster FS, Pavlin CJ, Harasiewicz KA, Christopher DA, Turnbull DH. Advances in ultrasound biomicroscopy. Ultrasound Med Biol 2000c;26:1–27.

Foster FS, Pavlin CJ, Lockwood GR, et al. Principles and applications of ultrasound backscatter microscopy. IEEE Trans Ultrason Ferroelec Freq Control 1993;40:608–617.

Goertz DE, Christopher DA, Yu JL, et al. High frequency color flow imaging of the microcirculation. Proceedings of the IEEE International Ultrasonics Symposium, 1998; 1525–1528.

Goertz DE, Christopher DA, Yu JL, et al. High-frequency colour flow imaging of the microcirculation. Ultrasound Med Biol 2000;26:63–71.

Hrabe de Angelis MH, Flaswinkel H, Fuchs H, et al. Genome-wide, large-scale production of mutant mice by ENU mutagenesis. Nature Genet 2000;25:444–447.

Kaufman MH. The atlas of mouse development. Toronto: Academic Press, 1999.

Kruse D, Fornaris J, Silverman R, Coleman D, Ferrara KW. A swept-scanning mode for estimation of blood velocities in the microvasculature. IEEE Trans Ultrason Ferroelec Freq Control 1998;45: 1437–1440.

Liu A, Joyner AL, Turnbull DH. Alteration of limb and brain patterning in early mouse embryos by ultrasound-guided injection of Shh-expressing cells. Mech Dev 1998;75:107–115.

Lockwood GR, Turnbull DH, Christopher DA, Foster FS. Beyond 30 MHz: Applications of high frequency imaging. IEEE Eng Med Biol 1996:60–71.

Marshall E. The rise of the mouse: Biomedicines model mammal. Science 2000;288:248–257.

Mor-Avi V, Korcarz C, Fentzke RC, et al. Quantitative evaluation of left ventricular function in a transgenic mouse model of dilated cardiomyopathy with 2-dimensional contrast echocardiography. J Am Soc Echocardiog 1999;12:209–214.

Passmann C, Ermert H. 150 MHz in vivo ultrasound of the skin: Imaging techniques and signal processing procedures. IEEE Ultrason Sympos 1994:1661–1664.

Pavlin CJ, Foster FS. Ultrasound biomicroscopy of the eye. New York: Springer-Verlag, 1995.

Scherrer-Crosbie M, Steudel W, Hunziker PR, et al. Determination of right ventricular structure and function in normoxic and hypoxic mice: A transesophageal echocardiographic study. Circulation 1998;98:1015–1021.

Scherrer-Crosbie M, Steudel W, Ullrich R, et al. Echocardiographic determination of risk area size in a murine model of myocardial ischemia. Am J Physiol 1999;277:H986–H992.

Sherar MD, Foster FS. The design and fabrication of high frequency poly(vinylidene fluoride) transducers. Ultrason Imaging 1989;11: 75–94.

Sherar MD, Starkoski BG, Taylor WB, Foster FS. A 100 MHz B-scan ultrasound backscatter microscope. Ultrason Imaging 1989;11:95–105.

Silverman RH, Reinstein DZ, Raevsky T, Coleman DJ. Improved system for sonographic imaging and biometry of the cornea. J Ultrasound Med 1997;16:117–124.

Srinivasan S, Baldwin HS, Aristizabal O. Noninvasive in utero imaging of mouse embryonic heart development using 40 MHz echocardiography. Circulation 1998;98:912–918.

Turnbull DH. In utero ultrasound backscatter microscopy of early stage mouse embryos. Comput Med Imaging Graphics 1999;23:25–31.

Turnbull DH, Bloomfield TS, Foster FS, Joyner AL. Ultrasound backscatter microscope analysis of early mouse embryonic brain development. Proc Natl Acad Sci 1995;92:2239–2243.

Turnbull DH, Ramsay JA, Shivji GS, et al. Ultrasound backscatter microscope analysis of mouse melanoma progression. Ultrasound Med Biol 1996;22:845–853.